Journal of Sound and Vibration (2000) **229**(3), 579–605
doi:10.1006/jsvi.1999.2517, available online at http://www.idealibrary.com on IDEAL®

SHOCK SPECTRAL ANALYSIS OF ELASTIC SYSTEMS IMPACTING ON THE WATER SURFACE

A. Carcaterra, E. Ciappi, A. Iafrati and E. F. Campana

INSEAN-Istituio Nazionale per Studi ed Esperienze di Architettura Navale, Via di Vallerano, 139, 00128, *Roma, Italy*

(*Received* 13 *April* 1999, *and in final form* 30 *July* 1999)

In this paper, the hydrodynamic and elastic forces arising in simple discrete and continuous systems impacting on the water surface are investigated. Both the impact of a single rigid wedge and the case of two elastically coupled bodies, where the lower one is wedge directly plunging the water, are studied. The analysis is performed by a simplified theoretical model and by a numerical simulation of the fluid–structure interaction. The concepts of residual and overall shock spectrum of the slamming force are introduced. The attention is then addressed to the case of a continuous flexural system. By an envelope analysis of the displacement response, related to the hydrodynamic force spectrum, a slamming shock spectral expansion is introduced. This model is able to provide some insight into the structural response during the impact. The characteristic maxima in the time histories of the elastic deformation are theoretically evaluated in terms of the impact quantities, such as the deadrise angle of the wedge, the entry velocity and the structural parameters. Results obtained by numerical simulations validate the theoretical predictions.

1. INTRODUCTION

The design of modern high-speed vessels makes it clear that extreme care must be devoted to fluid–structure interaction problems. In particular, dangerous impact phenomena occur in fast marine vehicles, leading to severe pressure load conditions of the hull structure. The prediction of the pressure and structural stress are of paramount importance, providing the tools for a better safety in ship design. This topic belongs to hydroelasticity theory, particularly developed in ship science, and illustrated in some fundamental works by Bishop and Price [1], Bishop *et al.* [2], Price *et al.* [3], Korobkin [4] and Faltinsen [5].

In spite of the scientific and technical interest for this topic and some remarkable works produced in this field, a full understanding of this complex impact phenomenon is still missing.

Nevertheless, some basic phenomena occurring during the impact process are well recognized. In fact, simple considerations show that, even though the water is usually treated as incompressible, water compressibility effects are of some importance

0022-460X/00/030579 + 27 $35.00/0

in the early stage of the contact. Actually, the intersection between the body and the free surface expands with a velocity that strongly depends on the body's shape. For a cylindrical body, impacting parallel to the free surface, the wetted area is bounded by two lines that move along the body surface with a velocity depending on the local deadrise angle. For flat-bottom profiles, this velocity may become very large and sometimes even larger than the speed of sound in water. In such a case, the contact body surface acts as a supersonic source disturbance, implying that a compressible model should be employed to describe the fluid dynamics of the impact.

In this context, Skalak and Feit [6], by using the acoustic approximation, determined the pressure distribution and the total hydrodynamic force for a semi-infinite wedge entering the water with a constant drop velocity. Using the same basic assumptions, Korobkin [7] developed a general theory for the compressible stage of the impact, providing a closed-form solution for parabolic profiles and a solution by quadratures for a large class of contours.

However, even when a first supersonic edge condition initially holds, a second subsonic stage of the impact occurs, due to the combined effect of velocity reduction and possible increase of the deadrise angle. The edge velocity becomes subsonic and an essentially incompressible stage takes place. Rather simple but effective models to study the problem were introduced by Von Karman [8] and Wagner [9], by assuming that the velocity field around the wetted part of the wedge can be approximated by that around an expanding flat plate. The Von Karman model considers a flat free surface while the Wagner approach accounts for a free surface deformation leading to a more reliable result.

More recently, the water entry problem has been analyzed by a numerical approach by Zhao and Faltinsen [10]. Through a boundary element formulation, they simulated the flow around a wedge for different values of the deadrise angle. In view of the extension to three-dimensional problems, the model has been successively applied to axisymmetric bodies [11]. In a recent work, Xu *et al.* [12] considered the problem of an axisymmetric vessel impact.

The problem of the structural response to the slamming load has been studied by several authors by both theoretical and numerical approaches. Recent works on the subject are those of Kim *et al.* [13] and Kalsvold and Faltinsen [14] in which the impact of a two-degrees-of-freedom (d.o.f.) elastic system and that of a beam are considered respectively.

In the above presentation, other occurring phenomena, such as the surface tension and air cushion, may be considered. Although affecting the fluid dynamic solution, surface tension does not change significantly the hydrodynamic load. On the contrary, for rather flat bottom geometries impacting on a rough sea, the air trapping may sensibly affect the pressure distribution and, thus, the total load on the hull. A survey on the subject is provided by Korobkin and Pukhnachov [4].

Most of the works developed in hydroelastic impact account for a constant entry velocity. In such a case, the hydrodynamic force on the body entering the water is, at least at an early stage of the impact, a quantity increasing with respect to time: in fact, the velocity is constant but the wetted area increases and it is responsible for the hydrodynamic force growth. Moreover, most of the scientific literature provides the results of the hydroelastic impact by using numerical tools. Although this

analysis provides accurate results even for complex systems, generally a full understanding on how each parameter plays its role in the phenomenon is not easily recovered by numerical simulations.

In the present paper, a different point of view of hydroelastic impact is introduced, aimed at finding closed-form relationships providing the maximum structural elastic response in terms of the whole set of impact parameters. In this frame, the body velocity reduction during the impact plays a key role in the maximum elastic response. The sudden velocity decreasing when the structure hits the water surface, tends to reduce the hydrodynamic force, while an opposite effect is due to the wetted increasing area. In the first stage the second effect is dominant; in the second short stage the two opposite phenomena find a balance and in the third stage the first effect definitely prevails. This leads to a characteristic time history of the hydrodynamic force. Initially it grows very fast; then a characteristic maximum peak follows and finally it decays.

The shock nature of this finite energy signal has here suggested the use of special and fruitful tools of analysis. One of these is certainly the shock spectrum. In fact, for finite energy input signal injected into a linear system, it provides the maximum of the output as a function of the system natural frequency. Moreover, this results is found without a direct solution of the problem; thus it seems to be a potentially attractive approach.

This results can be achieved only when a sharp characterization of the input force is available. Thus, a suitable simplified hydrodynamic model is also proposed and the impact force spectrum is determined in closed form. A systematic comparison is also made with a numerical model that fully accounts for free surface effects and non-linear hydroelastic interaction and with experimental results.

In the following a shock-spectral approach to water impact is systematically stated, dealing with a simple one-mode system and a multi-modal structure. The result seems to be promising, since the proposed method presents the following characteristics:

— not a direct solution of the problem is needed; this allows to recognize directly the effect of each parameter on the structural response and some simple interaction principles clearly arise;
— the method can be employed for wide parametric analyses, e.g., in order to find optimal design of the impacting system, since it does not require to develop each time a direct solution of the problem. This fact is relevant because numerical simulations of the hydroelastic coupled problem are extremely heavy, especially in view of parametric investigations;
— following the outlined procedure for a multi modal system (plate case) it is not difficult to generalize the approach to more complicated structures, eventually described by a finite element model.

These reasons seem to provide a good motivation for attempting this new approach to the water shock.

The basic result presented in the paper concerns the derivation of simple closed-form relationships that predict the value of the physical quantities, as the entry velocity, carried out impacting masses, the stiffness of the elastic connection

(or thickness, length and elastic constant for a flexural system), the deadrise angle that lead to a "dangerous" elastic response, i.e., to a maximum of the elastic force and stress. This particular combination of parameters is referred to in the following as "critical condition", which is determined in the paper under some particular assumptions.

The simpler considered system consists of two masses, where the lower one is a rigid wedge directly impacting the water. The attention is focused on the incompressible stage and, for this reason, the deadrise angle is chosen large enough to avoid supersonic edge conditions.

The study is carried out by using both a theoretical approach and a numerical model able to provide the slamming force.

The theoretical model is based on a simplified representation of the hydrodynamic force in terms of the actual depth and drop velocity of the impacting body. The study of the impact of the single wedge provides an analytical solution of the problem that turns to be useful for the theoretical prediction of the occurrence of critical conditions in the case of impact of an elastic system. In fact, a general analysis can be performed by using the concept of shock spectrum that leads to some general properties of the water impact force.

A second mathematical model is provided for the analysis of a wedge with elastic sides, flexurally deforming (plates). In such a case, a convenient closed-form spectral solution is provided. By using the hydrodynamic load determined for the rigid wedge case, both an inertial and a travelling pressure load are applied to the dropping plate.

In order to provide a characteristic relationship between hydrodynamics and structural response, the envelope of the time history at each plate location is determined by using the Hilbert transform. Its maximum is then evaluated by a generalization of the slamming shock spectrum concept, by eliminating the time dependence. The obtained spectral expansion is then modified by a suitable use of the Schwarz inequality that also allows for the elimination of the space dependence. Finally, a dimensionless form of the maximum envelope response leads to a simple spectral expansion in terms of the main parameters involved in the impact phenomenon.

The theoretical analysis is compared with some numerical results. In this case the solution of the hydrodynamic problem is obtained by a boundary element formulation that solves the Laplace equation in terms of the velocity potential in a way similar to that proposed by Zhao and Faltinsen [10] but here accounting both for a variable velocity and the hydroelastic coupling. A comparison is also made with the experiment described in reference [13].

The theoretical model employed for the cases of a single wedge and of a 2 d.o.f. elastic system is discussed in the next section, while in section 3 the mathematical formulation for continuous structures is presented. Finally, the boundary element numerical model to predict the hydrodynamic force is described in section 4.

2. THE HYDRODYNAMIC FIELD: AN APPROXIMATE SOLUTION

In this section, a simplified theoretical model for predicting the slamming force time history for a wedge plunging the water surface is proposed with applications to the rigid-body case and to simple elastic systems.

Although more sophisticated models can be developed to deal with water entry problems [10–12, 15] and a modified version of these is detailed in section 4 (accounting for a variable velocity and the hydroelastic interaction), the chance of determining an explicit parametric dependence of the hydrodynamic force on the quantities involved in the impact phenomenon is of fundamental importance in the analysis of the present problem.

Following an approach developed in references [16, 17], the present method allows for a simple analysis of the impact phenomenon leading to the analytical estimate of two basic quantities: the maximum slamming force F^* and the characteristics time delay t^* between the initial instant of the impact and the instant at which the force peak occurs. F^* affects directly the amplitude of the structure response, while t^* controls the peak frequency of the hydrodynamic force spectrum.

The hydrodynamic force acting on a massive wedge follows a characteristic evolution. On the one hand, the drop velocity decay causes a reduction of the slamming pressure while, at the same time, the wetted length increases. In the first stage of the impact, the latter effect dominates over the former and an increasing trend of the force is observed. At t^* the two opposite phenomena find a balance and a characteristic maximum is reached. Successively, the velocity reduction prevails against the increase of the wetted length and the slamming force definitively decays.

Let us consider a two-dimensional wedge of mass m per unit length, impacting on the water surface with an initial drop velocity v_0. The equation of motion simply reads $m\ddot{\zeta} + F_h = 0$, where F_h and ζ are the hydrodynamic force (per unit length) and the depth respectively.

By simple considerations, based on the momentum conservation, the following expression for the hydrodynamic force is obtained [8, 18]: $F_h = \eta\rho v_0^3 t$. The η coefficient is a function of the deadrise angle β of the wedge. Its expression has been derived by several authors using theoretical analysis or numerical computations. Following the approach of Von Karman [8] or Wagner [9] (approximating the flow about the entering wedge with the flow around a flat plate) η takes the form $\eta = \pi\gamma/\tan^2\beta$, where $\gamma = 1$ or $\pi^2/4$ respectively. More sophisticated models, as those developed by Vorus [15], Zhao and Faltinsen [10] and Dobrovol'skaya [19], reveal that γ is a function of the deadrise angle. Hence, the hydrodynamic force is expressed by

$$F_h = \pi\rho\gamma(\beta)\, v_0^3 t/\tan^2\beta.$$

In the present analysis, the estimate of γ, obtained in [10] by the similarity approach [19], is used.

It is interesting to notice that if μ is the added mass, the hydrodynamic force can be written as $F_h = \mathrm{d}/\mathrm{d}t(\mu v_0)$. By a direct comparison of the two last expressions of the force, $\mu = \rho\,(\pi/2)\,(\sqrt{\gamma(\beta)}\, v_0 t/\tan\beta)^2$. Now, the added mass of a flat plate of length L is $\rho(\pi/2)\, L^2$, and then it is natural to interpret μ as the added mass of a plate of length $\sqrt{\gamma(\beta)}\, v_0 t/\tan\beta$. Since $v_0 t/\tan\beta$ is the length corresponding to the geometric intersection between the wedge and the unperturbed free surface, $\sqrt{\gamma(\beta)}$ can be interpreted as a correction factor providing an estimate of the length over which the hydrodynamic load acts.

To estimate the typical maximum of the hydrodynamic force, a model accounting for the velocity decay must be necessarily introduced. When a variable drop velocity is considered, a reasonable approximation for the hydrodynamic force can be used:

$$F_h(\zeta, \dot{\zeta}) = \frac{\pi\rho\gamma}{v_0 \tan^2\beta}\, \dot{\zeta}^3 \zeta, \tag{1}$$

where the term v_0^3, appearing in the Wagner solution, is replaced by $\dot{\zeta}^3$. Moreover, in view of a closed-form solution, the direct dependence of F_h on time is eliminated by letting $t = \zeta/v_0$.

With these assumptions, the equation of motion becomes

$$\ddot{\zeta} + A\dot{\zeta}^3\zeta = 0, \quad \text{where } A = \frac{\pi\rho\gamma}{mv_0 \tan^2\beta}. \tag{2}$$

This non-linear equation admits an analytical solution that can be obtained by introducing a variable transformation and solving the resulting equation by separation of variables, leading to [7]

$$\dot{\zeta} = \frac{2v_0}{2 + Av_0\zeta^2}, \quad F_h(\zeta) = mA\dot{\zeta}^3\zeta = mA\left(\frac{2v_0}{2 + Av_0\zeta^2}\right)^3 \zeta. \tag{3}$$

Starting from equation (3), it is possible to obtain the relative maximum F^* of $F_h(\zeta)$ and the time t^* at which it occurs. In fact, from the solution of the algebraic equation $\mathrm{d}F_h/\mathrm{d}\zeta = 0$, it follows that

$$F^* = F_h(\zeta^*) = \left(\frac{5}{6}\right)^3 \sqrt{\frac{2\pi}{5}\ \rho\gamma m}\, \frac{v_0^2}{\tan\beta}, \qquad t^* = t(\zeta^*) = \frac{16}{15}\sqrt{\frac{2m}{5\pi\rho\gamma}}\, \frac{\tan\beta}{v_0}, \tag{4}$$

where ζ^* is the depth at which the maximum occurs.

It is interesting to note that ζ^* is simply related to t^*, actually $\zeta^* = \frac{15}{16} v_0 t^*$, indicating that, although responsible for the relative maximum of the slamming force, only a small reduction of the entry velocity occurs up to t^*.

A useful relationship between F^* and t^* can be also determined. In fact, simple mathematics leads to $F^*t^* = \frac{20}{81} mv_0 \approx 0{\cdot}247\, mv_0$, that is used in the following.

These results solve completely the problem related to the simple model represented by equation (2). Their use in predicting the response of the elastic system is discussed in the next section.

To validate the theoretical formulation, a comparison with an experiment described in reference [13] is performed. The test case refers to a wedge with a deadrise angle of 23°, a mass per unit length of 398 kg and an initial drop velocity $v_0 = 6{\cdot}9$ m/s. The theoretical prediction of the vertical acceleration is in good agreement with the experimental data (Figure 1).

Although this simple approach provides the hydrodynamic force, the actual pressure distribution is still unknown. However, it must be computed when considering a continuously deforming system. In fact, although several simplification hypotheses will be introduced in the next section for the plate water

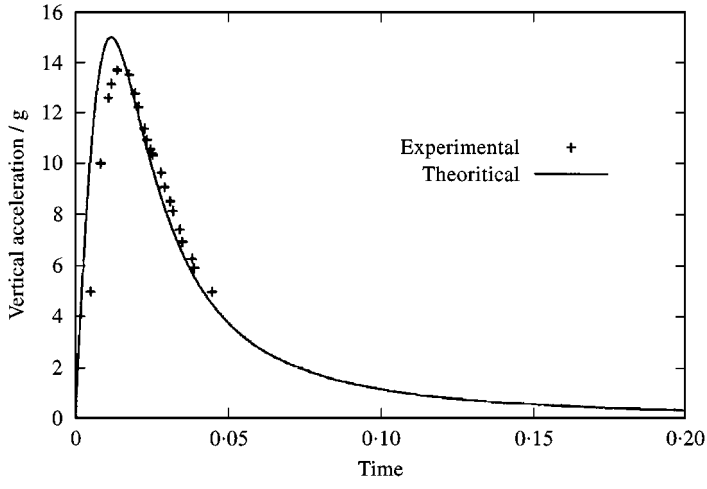

Figure 1. Comparison between the theoretical and the experimental vertical acceleration versus time. + , experimental; ——, theoretical.

entry, that do not involve directly the pressure field, it must be determined to provide comparisons between theoretical and numerical results.

Zhao and Faltinsen [10] demonstrated that, following the theory of matching asymptotic expansion, it is possible to determine a composite solution for the pressure distribution around a wedge when a constant drop velocity and small deadrise angles are considered. In this procedure, the flow field is divided into an outer and an inner region. The former is solved by the above-mentioned expanding flat plate approximation [9], that provides the wetted length $c(t)$, i.e., the length of the portion of the wedge side directly in contact with the water, bounded by the intersection point between the body and the free surface. In the latter region, close to the edge of the wetted area, the details of the jet flow around the abscissa $c(t)$ are analyzed.

The pressure field is given by

$$p = \begin{cases} v_0 c\dot{c}(c^2 - x^2)^{-1/2} - \rho v_0 c\dot{c}(2c(c-x))^{-1/2} + 2\rho\,\dot{c}^2|\tau|^{1/2}(1+|\tau|^{1/2})^{-2}, \\ \qquad \text{for } 0 \leqslant x \leqslant c, \\ 2\rho\dot{c}^2|\tau|^{1/2}(1+|\tau|^{1/2})^{-2} \\ \qquad \text{for } x > c, \end{cases}$$

where $c = (\pi/2)\, v_0 t/\tan\beta$, $\dot{c} = (\pi/2)\, v_0/\tan\beta$. Moreover, the parameter τ appearing in the previous relationships varies from 0 to ∞, and is related to the abscissa x by

$$x - c = \frac{\delta}{\pi}\,(-\ln|\tau| - 4|\tau|^{1/2} - |\tau| + 5).$$

These results hold for a constant entry velocity.

To account for the velocity decay, the pressure field can be rearranged by letting $c = \sqrt{\gamma\zeta}/\tan\beta$, consistent with the approximation made on the hydrodynamic force.

With these positions an approximate pressure distribution is obtained. However, the integral of this pressure field over the estimated wetted length leads to an hydrodynamic force similar to that obtained by the approximate analysis developed in the first part of this section, and by the boundary element model described in section 4.

3. A SHOCK SPECTRAL APPROACH TO WATER SLAMMING

In this section, the analysis of the response of an elastic impacting system is investigated.

A 2 d.o.f.s and a continuous flexural system are considered. The pulse nature of the slamming force, determined in the previous section, suggests an approach to the problem by using the shock spectrum theory. The simpler discrete elastic system leads to the concept of the *slamming shock spectrum* whose dimensionless form allows for the prediction of the occurrence of critical conditions, as described in section 3.1.

The behaviour of the elastic flexural system is more difficult and requires more sophisticated mathematical tools. However, even in this case, a serial expansion in terms of modal shock spectra is provided in section 3.2, once a suitable use of the Hilbert envelope and of the Schwarz inequality is made, providing the *slamming shock spectral series.*

3.1. TWO DEGREES-OF-FREEDOM SYSTEM

A simple system is investigated here, consisting of two elastically coupled bodies of mass m_1 and m_2. The lower one, a rigid wedge with mass m_1, directly impacts the water, while the upper is suspended over the first one by a spring of stiffness k.

Although this is an elementary structure, it can be investigated as a prototype system whose behaviour reveals important characteristics of the structural water shock response. An interesting analysis of the impacting oscillator can be found in a recent work of Kim *et al.* [13].

The search for the critical condition of the impacting 2 d.o.f.s oscillator is proposed. For example, it could be requested to predict, when existing the critical value of the stiffness k, i.e., the value that leads to the maximum amplitude of the spring elastic force, once all the other impact parameters are given.

Since in the previous section the evaluation of the hydrodynamic force was obtained, it is interesting to study under which conditions this force is almost independent of the elastic force, i.e., when the motion of m_1 is substantially not affected by m_2. In such a case the hydrodynamic force analysis, developed in section 2, can still be considered valid.

Let us introduce, for simplicity, the non-dimensional parameters $\sigma = \rho v_0^2/k$ and $\delta = m_2/m_1$. When the elastic force F_e satisfies the condition $F_e \ll F_h$, its effect on F_h is negligible. In terms of the non-dimensional parameters, this situation implies the condition $\sqrt{\sigma/\delta} \gg \tan\beta$. Hence, the suspended mass behaves like a mass on

a foundation that receives a known shock acceleration of the form $F_h(t)/m_1$, where $F_h(t)$ is determined in section 2.

In this case, the shock spectrum technique can be profitably used to predict the maximum response of the suspended mass as a function of the natural frequency $f_n = 1/(2\pi)\sqrt{k/m_2}$ of the system itself. The residual shock spectrum $S(f_n)$ represents the maximum response of the system for $t > T$, where T is the time duration of the shock waveform, i.e., the maximum amplitude of the vibration response when a stationary oscillation is reached [20, 21]. $S(f_n)$ is related to the Fourier transform $\mathscr{F}$ of the shock signal by the following relationship:

$$S(f_n) = 2\pi f_n |\mathscr{F}(f_n)|. \tag{5}$$

Even though equation (5) could be directly employed to provide the shock spectrum once the hydrodynamic force is known, a more general and even simpler result can be obtained by introducing a suitable non-dimensional form of the hydrodynamic load. If relations (4) are rewritten in terms of the following non-dimensional variables: $\tilde{t} = t/t^*$, $\tilde{\zeta} = \zeta/\zeta^*$, $\tilde{F}_h = F_h/F^*$, the hydrodynamic force takes the form

$$\tilde{F}(\tilde{t}) = \frac{81}{20v}\left[\frac{2}{2+\tilde{\zeta}^2/v}\right]^3 \tilde{\zeta}, \qquad v = \frac{m}{\rho(v_0 t^*)^2}\frac{\tan^2\beta}{\pi\gamma(\beta)} \equiv \frac{5}{2}\left(\frac{15}{16}\right)^2. \tag{6}$$

Equation (6) reveals that the slamming force is invariant with respect to the impact parameters when this particular non-dimensional form is chosen. This allows an analysis that is not case dependent and the spectral properties of the slamming force can be investigated once for all by using the previous equation. The shock spectrum of the force

$$\tilde{S}_{RES}(\tilde{f}_n) = 2\pi\tilde{f}_n |\tilde{\mathscr{F}}\{\tilde{F}_h\}| \tag{7}$$

is represented in Figure 2 versus the non-dimensional frequency $\tilde{f}_n = f_n t^*$. The actual elastic force can be determined by multiplying the residual shock spectrum by the maximum hydrodynamic force F^* and by the mass factor $\delta = m_2/m_1$. By direct inspection of the shock spectrum curve, it appears that the relative maximum occurs at $\tilde{f}_n \cong 0{\cdot}2$ and, hence, the critical frequency can be estimated as $\tilde{f}_{cr} = (f_n t^*)_{cr} = 0{\cdot}2$.

The asymptotic residual response does not provide the maximum vibrational amplitude of the system during the transient excitation (i.e., when $t < T$). To this end the overall shock spectrum must be computed. This requires the direct evaluation of the absolute maximum of the elastic response. Even in this case a single characteristic overall spectrum is determined, capable of dealing with any impact condition. By using the non-dimensional quantities introduced earlier one has for the elastic force,

$$\tilde{F}_e(\tilde{t}, \tilde{f}_n) = \int_{-\infty}^{+\infty} 1/[1-(\tilde{f}/\tilde{f}_n)^2]\ \tilde{\mathscr{F}}\{\tilde{F}_h\}\, e^{2\pi j \tilde{f}\tilde{t}}\, d\tilde{f}.$$

Thus, the slamming overall shock spectrum is

$$\tilde{S}_{OV}(\tilde{f}_n) = \max\{\tilde{F}_e(\tilde{t}, \tilde{f}_n)\}, \quad 0 \leqslant t < \infty.$$

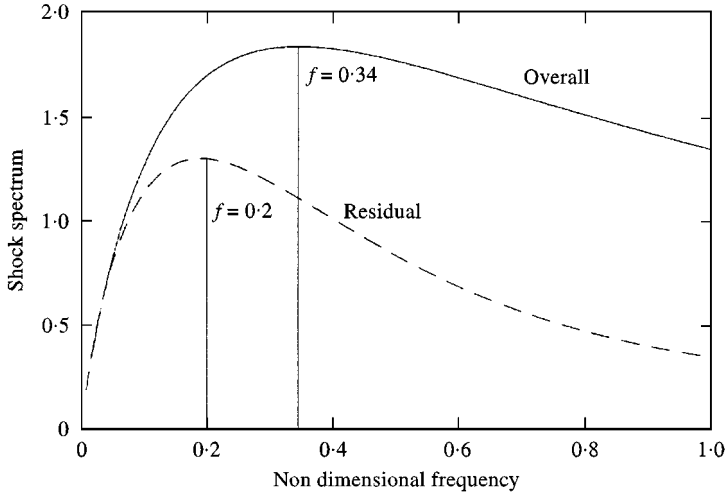

Figure 2. Shock spectrum of the hydrodynamic force versus the non-dimensional frequency.

Again the actual elastic force is determined as a function of the amplitude factor $F^*\delta$. This characteristic function has been evaluated and plotted in Figure 2. Its relative maximum falls in correspondence of $\tilde{f}_{cr} = (f_n\, t^*)_{cr} = 0{\cdot}34$.

The determined conditions $\tilde{f}_{crRES} = 0{\cdot}2$ and $\tilde{f}_{crOV} = 0.34$ have a general nature and can be employed for the prediction of the critical values of any of the parameters involved in the impact phenomenon. In fact, by making explicit the expression of t^* given in section 2, and the expression of f_n, one has

$$(f_n\, t^*)_{cr} = \tilde{f}_{cr} \quad \Rightarrow \quad \left(\frac{\tan\beta}{\sqrt{\gamma(\beta)}}\,\frac{1}{\sqrt{\sigma\delta}}\right)_{cr} = \frac{15\pi}{8}\sqrt{\frac{5\pi}{2}}\,\tilde{f}_{cr}$$

that allows one to compute the critical values of the required dimensionless parameters once the others are given. This relationship provides a general answer to the question proposed at the beginning of this section.

If one is interested in the critical value, e.g., of the elastic constant k, after simple mathematics the parameter σ_{cr} is determined, i.e.,

$$\sigma_{crRES} = \frac{25}{4\pi^3}\,\frac{1}{\delta v}\,\frac{\tan^2\beta}{\gamma}, \quad \sigma_{crOV} = \frac{8{\cdot}16}{4\pi^3}\,\frac{1}{\delta v}\,\frac{\tan^2\beta}{\gamma} \tag{8}$$

and thus

$$k_{cr} = \frac{\rho v_0^2}{\sigma_{cr}}. \tag{9}$$

It is clear that a complete set of critical values of the impact variables can be derived besides k_{cr}, i.e., a critical velocity, deadrise angle, suspended and impacting mass.

It is apparent that, in correspondence with the critical condition, the maximum elastic force has the same order of magnitude as that of the hydrodynamic one, being $\tilde{S}_{RES}(\tilde{f}_{cr}) \approx 1{\cdot}3$, $\tilde{S}_{OV}(\tilde{f}_{cr}) \approx 1{\cdot}8$, at least if the mass factor δ is of unit order of magnitude. Therefore, in that case, it can be concluded that the initial assumption $F_h \gg F_e$ does not strictly hold. In this case, a strong coupling between hydrodynamic and elastic force is expected. However, this does not affect sensibly the estimate of the critical frequency and even the maximum of the elastic force agrees quite satisfactorily with the numerical results. On the contrary, when δ is small, the analysis is valid in the whole frequency range.

In order to test these results, several impact simulations were performed by varying the values of k and of σ. The mass ratio is $\delta = 1$, while the deadrise angle is 10° and the corresponding γ is 2·2. The choice $\delta = 1$ is aimed to perform the comparison even when $F_h \simeq F_e$.

First the hydrodynamic force is determined via numerical simulation based on a boundary element discretization of the free surface, whose details are given in section 4. This force is directly applied to the impacting mass and the coupled hydroelastic equations are solved. The maxima of the elastic force obtained for each elastic force time history, corresponding to different values of σ, are plotted in Figure 3. The same simulations are performed by using the hydrodynamic force expression derived in section 2, and a good agreement is shown in Figure 3. The shock spectra provide *a priori* the critical values $\sigma_{OV} \cong 0{\cdot}00042$ and $\sigma_{RES} \cong 0{\cdot}00135$. The numerical simulation finds $\sigma \cong 0.0008$ that falls into the interval $[\sigma_{OV}, \sigma_{RES}]$. It is a quite good result especially considering that, in that region, the curve appears to be rather flat.

3.2. CONTINUOUS FLEXURAL STRUCTURE

In this section, some general properties of the elastic response of a wedge consisting of two elasticity deforming sides are investigated. The technique is based

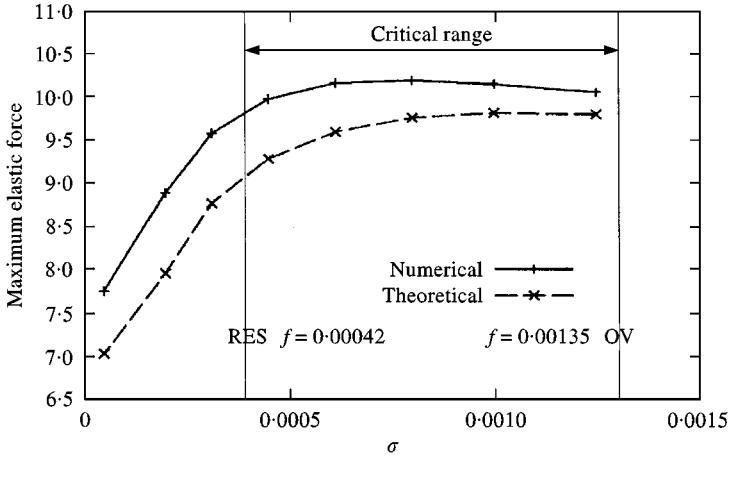

Figure 3. Maxima of the elastic force versus σ: —+—, numerical; – × –, theoretical.

on the idea of a shock spectral approach that is carried on by using the Hilbert envelope [22], the Schwartz inequality and some results of the previous section.

More precisely, the theoretical analysis of the structural response follows the steps listed below:

- statement of the basic governing equations,
- analysis of the time-domain Hilbert envelope,
- application of the Schwarz inequality and definition of the *water shock spectral series*.

Some simplified hypotheses are accounted for:

(i) The structural deformation is small and does not affect the flow around the wedge. This implies that the motion of the centre of gravity of the wedge corresponds to the entry of a rigid body. Thus, the model developed in the previous section is still valid to predict the total force on the structure.

(ii) The effect of the added mass is neglected when considering conditions in which the wetted length is small with respect to the vibrating length of the plate. This allows to neglect the effects of the fluid inertia by studying the bending response of the plate.

Therefore, the added mass associated with the rigid-body motion is accounted for by the hydrodynamic model developed in section 2 and by the numerical solution given in section 4. The added mass related to the elastic deformation of the plate and the structure–fluid coupling are indeed neglected (i), (ii). These simplifications allow to determine the shock spectral approach capable of providing simple parametric dependencies of the bending moment on the impact quantities.

Further simplifications will be introduced during the derivation of the spectral solution and will be discussed later on.

The formal consequences of hypotheses (i) and (ii) are detailed in the following sections.

3.2.1. *Basic governing equation*

Following the scheme of Figure 4, let us introduce two different reference systems, $R_0(x_0, y_0, z_0)$ and $R_G(x_G, y_G, z_G)$, the first fixed on the water surface while the second, with axes parallel to those of the first, follows the wedge centre of gravity G.

Neglecting the three-dimensional hydrodynamic effects at the edges and using the result of section 2 and hypothesis (i), the motion of G is described by $m\ddot{\zeta}_G + F_h = 0$, where m is the total wedge mass per unit length along y_G and $\zeta_G(t)$ is the centre of gravity displacement with respect to R_0. The total mass consists of two contributions: the first $2m_p$ is the mass of the impacting flexural structure (consisting of two plates), while $2m_s$ is the carried mass. In the following developments, it is easier to express the total mass m in the terms of the mass of a single wedge side (m_p), i.e., $m = \alpha m_p$.

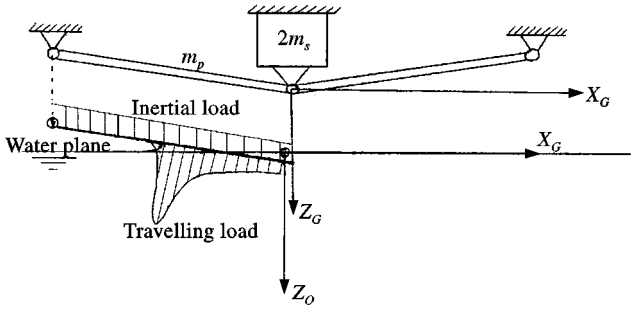

Figure 4. Structural model and reference systems.

The plate's structural model has to take into account the following effects: (i) a hydrodynamic pressure load p_w, moving along x with velocity v_e and (ii) an inertial uniformly distributed load on the plate, proportional to $\ddot{\zeta}_G$ (see Figure 3).

Assuming that each plate behaves as an infinite along y_G, according to the hydrodynamic model, the y_G co-ordinate disappears in the equation of motion. Taking advantage of the symmetry of the problem, it is possible to study only the elastic response of one wedge side. Moreover, in the following (as in section 2), we refer to a unit length along the y_G co-ordinate.

Let $\dot{\zeta}_e(x_G, t)$ be the relative elastic plate's deflection with respect to R_G. Therefore, the displacement $\zeta(x_0, t)$ of a plate's point $P(x_G, y_G)$ with respect to R_0 is $\zeta(x_0, t) = \dot{\zeta}_e(x_G, t) + \dot{\zeta}_G(t)$. Consequently, the plate's equation reads

$$D\frac{\partial^4 \zeta_e}{\partial x_G^4} + \rho_s h\frac{\partial^2 \zeta_e}{\partial t^2} = p_w - \rho_s h\frac{\partial^2 \zeta_G}{\partial t^2} = p, \tag{10}$$

where ρ_s is the material density, $D = Eh^3/12(1 - \nu_s^2)$ is the plate stiffness, E and ν_s being the Young's modulus and the Poisson ratio respectively and h the plate's thickness.

The equation of rigid-body motion allows to express $\partial^2\zeta_G/\partial t^2$ in terms of $F_h(t)$, known from section 2. In fact, the following relationship holds: $F_h(t) = m_p\alpha\partial^2\zeta_G/\partial t^2$, so that $\partial^2\zeta_G/\partial t^2 = F_h(t)/m_p\alpha$. On the other hand, the pressure field p_w is not simply recoverable. When a variable drop velocity is accounted for, a suitable expression of the pressure field can be found by substituting the actual drop velocity into the Wagner expression, as described in section 2. This approach will be used later to produce comparison results.

In the present section, aimed at studying in closed form the bending shock spectral properties, the hydrodynamic travelling pressure load is replaced by a moving rectangular pressure distribution, whose front is applied in correspondence with the end of the wetted length of the wedge. Moreover, the load is supposed to move at a constant speed v_e, while actually a weak decrement of it is predicted by the theory (see section 2).

The amplitude of the travelling pressure is simply obtained by its space-average at time t, i.e.,

$$p_w = \frac{F_h(t)}{2v_e t}W(x_G), \qquad W(x_G) = \begin{cases} 1 & \text{for } x_G \leqslant v_e t, \\ 0 & \text{for } x_G > v_e t. \end{cases}$$

In this way, the r.h.s. of equation (10) takes the simplified form

$$p(x_G, t) = F_h(t)\left[\frac{W(x_G)}{2v_e t} - \frac{1}{\alpha L}\right].$$

Let us express the plate elastic motion by a modal expansion, i.e., $\zeta_e(x_G, t) = \sum_{k=1}^{\infty} \Phi_k(x_G) q_k(t)$, Φ_k, q_k being the eigenfunctions and the normal co-ordinates respectively. The Lagrangian co-ordinates are recovered by solving the equations

$$\ddot{q}_k + \lambda_k^2 q_k = \int_0^L p(x_G, t)\, \Phi_k(x_G)\, \mathrm{d}x = I_k(t).$$

In the following, simply supported ends are considered and thus the eigenfunctions are simply harmonic. Although this is a particular case, the results obtained are significant for understanding some basic effects related to the slamming load on the structure. By using the determined expression of the pressure field, after some mathematics one has

$$I_k(t) = \sqrt{\frac{2}{m_p}}\frac{F_h(t)}{\pi k}\left(\frac{(-1)^k - 1}{\alpha} + \frac{L}{2v_e t}\left[1 - \cos\frac{\pi k v_e t}{L}\right]\right)$$

where $v_e = v_0\sqrt{\gamma}/\tan\beta$. Again the wetted length correction factor $\sqrt{\gamma}$ has been used. Starting from this expression, some relevant properties of the solution of the plate's equation can be predicted on the basis of the studied slamming shock spectrum.

3.2.2. *Structural response via the Hilbert envelope and Schwarz inequality*

The kth Lagrangian co-ordinate is determined by the convolution integral

$$q_k(t) = \frac{1}{\omega_k}\int_0^t I_k(\tau)\sin\omega_k(t-\tau)\,\mathrm{d}\tau$$

Since $F_h(t) = 0$, when $t < 0$, the lower limit of the integral can be substituted with $-\infty$. Moreover, the slamming force rapidly decays because of its pulse nature. In fact, from section 2 one has that

$$F_h(t) \approx 0 \quad \text{when } t > nt^* \quad \left(\text{if } n = 8 \rightarrow \frac{F_h(t)}{F^*} < 0{\cdot}1\right)$$

Therefore, when $t > nt^*$, the previous integral is replaced by

$$q_k(t) = \frac{1}{\omega_k}\int_{-\infty}^{+\infty} I_k(\tau)\sin\omega_k(t-\tau)\,\mathrm{d}\tau.$$

Let us now introduce the Hilbert transform H. The analytic signal associated with the kth generalized co-ordinate is $\hat{q}_k = q_k + \mathrm{j}H\{q_k\}$. The modulus of the analytic signal provides the so-called Hilbert envelope [22], that is actually the envelope of the time history of the signal itself. This analysis is extremely useful to cancel out the time dependencies of the system response while holding its maximum value.

By using some basic properties of the Hilbert operator (see Appendix A) it follows that

$$\hat{q}_k = -\frac{\mathrm{j}}{\omega_k}\,\mathrm{e}^{\mathrm{j}\omega_k t}\int_{-\infty}^{+\infty} I_k(\tau)\,\mathrm{e}^{-\mathrm{j}\omega_k\tau}\,\mathrm{d}\tau \;\Rightarrow\; \hat{q}_k = -\frac{\mathrm{j}}{\omega_k}\,\mathrm{e}^{\mathrm{j}\omega_k t}\,\mathscr{F}_k\{I_k(t)\}$$

where $\mathscr{F}_k$ denotes the Fourier transform of kernel $\mathrm{e}^{-j\omega_k t}$. Consequently, an analytic elastic displacement $\hat{\zeta}_e$ can be also defined as

$$\hat{\zeta}_e(x_G, t) = \zeta_e + \mathrm{j}\mathscr{H}\{\zeta_e\} = \sum_{k=1}^{\infty}\sqrt{\frac{2}{m_p}}\sin\frac{\pi k x_G}{L}\,\hat{q}_k(t). \tag{11}$$

The introduction of a dimensionless analysis is convenient. The plate's non-dimensional natural frequencies are $\tilde{f}_k = k^2\tilde{f}_1 = k^2(f_1 t^*)$, where f_1 is the first natural frequency of the structure. After some mathematics (see Appendix B) the non-dimensional analytic signal is obtained:

$$\frac{\hat{q}_k(\tilde{t})}{\sqrt{m_p}\,\zeta^*} = -\varepsilon\alpha\,\mathrm{j}\,\frac{\mathrm{e}^{2\pi\mathrm{j}k^2\tilde{f}_1\tilde{\tau}}}{2\pi k^2\tilde{f}_1}\,\tilde{\mathscr{F}}_k\{\tilde{I}_k\}, \tag{12}$$

where $\varepsilon = 64\sqrt{2}/243$ and

$$\tilde{\mathscr{F}}_k(\cdot) = \int_{-\infty}^{+\infty}(\cdot)\,\mathrm{e}^{-2\pi\mathrm{j}k^2\tilde{f}_1\tilde{t}}\,\mathrm{d}\tilde{t},$$

$$\tilde{I}_k = \frac{I_k}{F^*\sqrt{2/m_p}} = \frac{\tilde{F}_h(\tilde{t})}{\pi k}\left(\frac{(-1)^k - 1}{\alpha} + \frac{L}{4\tilde{f}_e\tilde{t}}[1 - \cos 2\pi k\,\tilde{f}_e\,\tilde{t}]\right)$$

where $\tilde{f}_e = v_e t/2L$. Therefore by substituting equation (12) into equation (11) the elastic beam deflection is expressed by

$$\tilde{\hat{\zeta}}_e(\tilde{x}, \tilde{t}) = \frac{\hat{\zeta}_e(\tilde{x},\ \tilde{t})}{\zeta^*} = -\sqrt{2}\,\varepsilon\,\alpha\,\frac{1}{2\pi\tilde{f}_1}\sum_{k=1}^{\infty} z_k\,\frac{\sin\pi k\tilde{x}}{k}$$

$$z_k = \mathrm{j}\,\frac{\mathrm{e}^{2\pi\mathrm{j}k^2\tilde{f}_1\tilde{t}}}{k}\,\tilde{\mathscr{F}}_k\{\tilde{I}_k\}, \quad \tilde{x} = \frac{x_G}{L}.$$

By separating the real and imaginary parts in the previous relationship one obtains

$$\frac{\hat{\zeta}_{eR,I}}{\zeta^*} = \sqrt{2}\varepsilon\alpha\,\frac{1}{2\pi f_1}\sum_{k=1}^{\infty} z_{kR,1}\,\frac{\sin\pi k\tilde{x}}{k}.$$

$\hat{\zeta}_{eR,I}$, $z_{kR,I}$ being the real (R) and the imaginary (I) parts of the corresponding complex quantities.

The application of the Schwarz inequality [23] allows one to write

$$\sum_{k=1}^{\infty} z_{kR,I}\,\frac{\sin k\pi\tilde{x}}{k} \leqslant \left[\sum_{k=1}^{\infty} z_{kR,I}^2\sum_{k=1}^{\infty}\frac{\sin^2 k\pi\tilde{x}}{k^2}\right]^{1/2}.$$

Moreover, the dependence on the dimensionless space co-ordinate can be suppressed by using the following inequality:

$$\sum_{k=1}^{\infty} \frac{\sin^2 k\pi\tilde{x}}{k^2} \leqslant \frac{\pi^2}{2}(1-\tilde{x})\tilde{x} \leqslant \frac{\pi^2}{8},$$

where the Fourier expansion of $(1-\tilde{x})\,\tilde{x}$ is performed. By combining the previous equations, the modulus of the dimensionless analytic displacement satisfies the final inequality:

$$|\tilde{\tilde{\zeta}}_e| \leqslant \frac{\pi}{2}\frac{\varepsilon\alpha}{2\pi\tilde{f}_1}\sqrt{\sum_{k=1}^{\infty}|z_k|^2}.$$

This is the condition holding for the Hilbert envelope of the elastic beam displacement with respect to the time variable. The written inequality is satisfied at any time and for any point along the plate.

This equation deserves some comments. It is important to note that both the time and space dependencies are suppressed and the terms on the r.h.s. actually depend only on the elastic and impact parameters of the problem. Therefore, we are now able to discuss the upper bound of the elastic residual displacement (by its envelope) in terms of the characteristic parameters of the problem, by a way analogous to that developed in section 2.

3.2.3. *Definition of the water shock spectral series*

The last step consists of further developments to provide the required spectral result in terms of the internal elastic force on the plate. In particular, the *water shock spectral series* is introduced. Let us approximate the analytic residual bending moment by

$$\hat{M}_B \approx \pi^2 \frac{D\hat{\zeta}_e}{L^2}. \tag{13}$$

After some mathematics and using the result of the previous section, the following expression is obtained (see Appendix C):

$$|\tilde{M}_B| = \left|\frac{\hat{M}_B}{p_0 L^2}\right| \leqslant 5\left(\frac{15}{16}\right)^2 \varepsilon\frac{\sqrt{\gamma}}{tg\,\beta}\bar{f}_e\sqrt{\sum_{k=1}^{\infty}\frac{\tilde{S}_k^2}{k^6}}, \qquad \tilde{S}_k = 2\pi\tilde{f}_k|\tilde{\mathscr{F}}_k(\tilde{I}_k)|, \quad p_0 = \frac{1}{2}\rho_w v_0^2,$$

where $\tilde{S}_k$, defined in analogy to the shock spectrum given in section 2, is the *water shock spectrum* modal component. This relationship provides the dimensionless bending moment $\tilde{M}_B$ in terms of the all the involved parameters, i.e., α, $\tilde{f}_1, \tilde{f}_e$ and β.

Although the explicit form of the spectral functions $\tilde{S}_k$ is obtained in Appendix *D*, its physical meaning is discussed below.

Two different spectral contributions play their role in the shock spectral components: the inertial slamming spectrum $\tilde{S}^{(I)}$ and the travelling slamming spectrum $\tilde{S}^{(T)}$:

$$\tilde{S}_k(\alpha,\tilde{f}_1,\tilde{f}_e) = \left|\frac{(-1)^k-1}{\pi\alpha k}\tilde{S}^{(I)}(\tilde{f}_k) + \frac{1}{4\pi k\tilde{f}_e}\tilde{S}^{(T)}(\tilde{f}_k) - \frac{1}{8\pi k\tilde{f}_e}\left[\frac{\tilde{S}^{(T)}(\tilde{f}_k+k\tilde{f}_e)}{1+\tilde{f}_e/(k^2\tilde{f}_1)} + \frac{\tilde{S}^{(T)}(\tilde{f}_k-k\tilde{f}_e)}{1-\tilde{f}_e/(k^2\tilde{f}_1)}\right]\right|. \tag{14}$$

They are complex functions, formally similar to the residual shock spectra of a known slamming signal.

The first, $\tilde{S}^{(I)}$, is just the residual shock spectrum of the slamming force $\tilde{F}_h$ as introduced in section 2, but in complex form because it does not involve the modulus of the Fourier transform (see Appendix D). It is related to the structural excitation induced by the inertial effect, i.e., by the sudden deceleration produced when hitting the water surface. Of course, each mode reacts to this excitation and the corresponding spectral contribution is represented by the first term on the r.h.s. of equation (14). It is obtained by the residual shock spectrum of the rigid body entry where the frequency argument is replaced by $\tilde{f}_k$ for each modal contribution. The second term on the r.h.s. of equation (14) accounts for of the travelling pressure load. $\tilde{S}^{(T)}$ is the complex residual shock spectrum of the signal $\tilde{F}_h/\tilde{t}$ that characterizes the spectral properties of a rectangular pressure distribution. Finally, the term in square brackets, simply obtained by shifting the travelling shock spectrum, is directly related to the speed of the pressure load that has also an effect on the structural response.

The residual and the overall shock spectra are represented in Figures 5 and 6 for both the inertial and the travelling load contributions.

It must be note that the moment associated with equation (14) is obtained in terms of residual vibrations with some approximations. Therefore, a direct comparison with the absolute maxima of the numerical simulations does not provide a completely satisfactory agreement. Since some information about the overall spectrum has been obtained in the previous analysis, this can be suitably introduced into expression (13). Thus the original spectral series is slightly modified, by introducing the average shock spectrum series leading to $|\tilde{M}|_{AV}$ defined as in Appendix E. The comparisons with numerical simulations are performed with this last quantity.

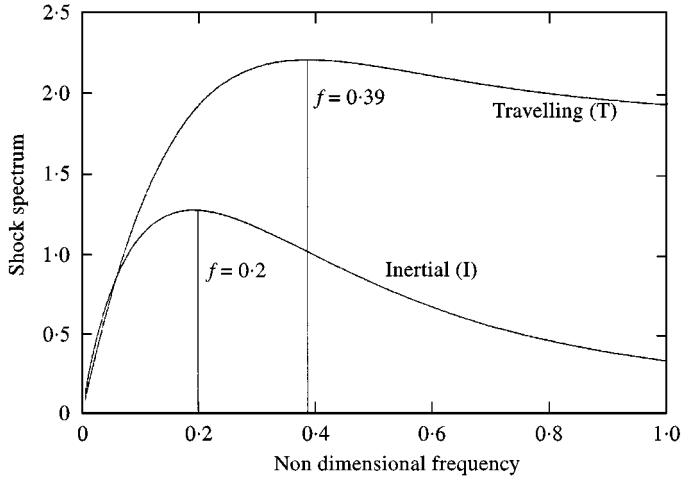

Figure 5. Residual shock spectrum for the inertial and the travelling load versus the non-dimensional frequency.

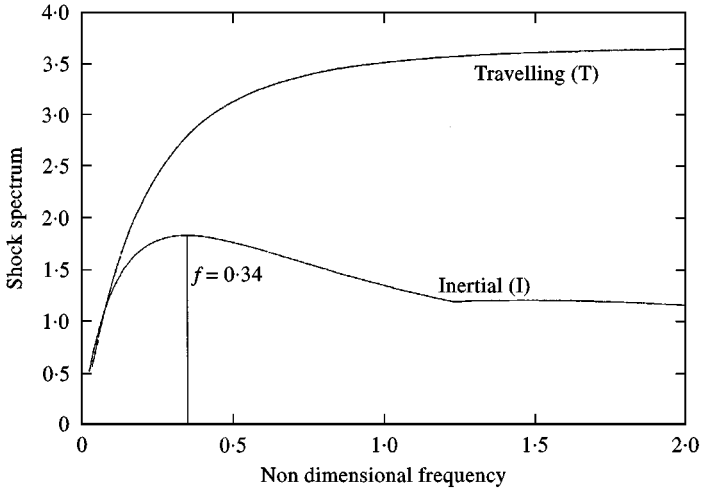

Figure 6. Overall shock spectrum for the inertial and the travelling load versus the non-dimensional frequency.

Therefore, the shock spectral series related to the bending moment is a function of four parameters only: $\alpha, \tilde{f}_1, \tilde{f}_e$ and β. This simplifies considerably the analysis of the impact problem and allows for the prediction of critical conditions in terms of simple and general relationship among the three dimensionless quantities. These conditions are investigated once and for all by analyzing the serial shock spectrum and the results can be easily translated in terms of the actual physical quantities involved in the phenomenon.

The expression provided reveals that when $\tilde{f}_e \to 0$, the travelling shock terms vanish and only the inertial shock term survives. Moreover, the presence of the $1/k^6$ factor in the spectral series guarantees a fast convergence of the series itself.

The developed analysis neglects the possible modification of the flow about the wedge due to the structural deformation.

This condition can be expressed in terms of the dimensionless variables of the problem. When $\tilde{f}_e \ll 1$ the plate–water interface is localized around the vertex line of the wedge and the local deformation is clearly associated with the plate slope θ at the vertex support. If $\theta \ll \beta$, it can be reasonably assumed that the water-flow is not affected by the structural deformation, i.e., the local deadrise angle is not sensibly modified during the impact.

Therefore, condition (i) previously introduced, finds a suitable translation in terms of the three dimensionless defined parameters. More precisely, it can be written in analytical form (see Appendix F) as

(i) $\zeta_e \ll \zeta_G \Rightarrow \tilde{f}_e |1 - \alpha \tilde{f}_e| \ll \tilde{f}_1$

besides the obvious one:

(ii) $v_e t^* \ll L \Rightarrow \tilde{f}_e \ll 1.$

Thus, the determined shock spectral series can be used correctly only under these constraints.

Some comparisons between numerical simulations and the results obtained by the shock spectral series are presented.

The direct numerical solution of equation (10) is determined. The pressure contribution to the external load has been determined by the Wagner theory [9] in which the velocity, assumed to be constant, is replaced by the actual drop velocity provided by equation (3). In Figure 7 a typical bending moment distribution is plotted versus time. Several simulations of the elastic response are obtained by varying $\tilde{f}_1$ and for each time history the maximum of the surface plotted in Figure 8 is kept. The results of this time-consuming analysis are compared with the fast shock spectral series prediction. Both curves refer to $\beta = 15°, \tilde{f}_e = 0{\cdot}16$. The same comparison is shown in Figure 9 and $\beta = 15°$, $\tilde{f}_e = 0{\cdot}25$. The agreement is quite good. In particular, the relative maxima in the bending moment are located at similar frequencies for the theoretical and the numerical predictions.

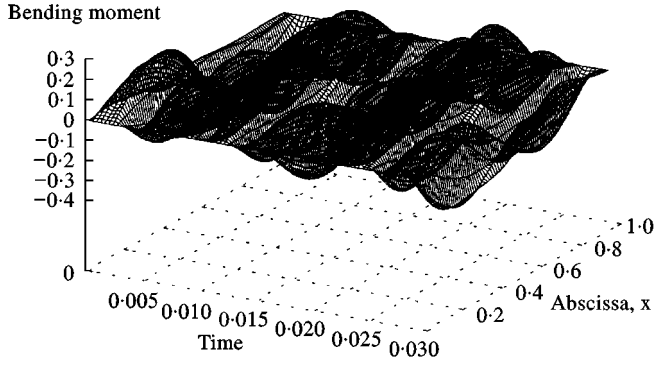

Figure 7. Time and space evolution of the bending moment.

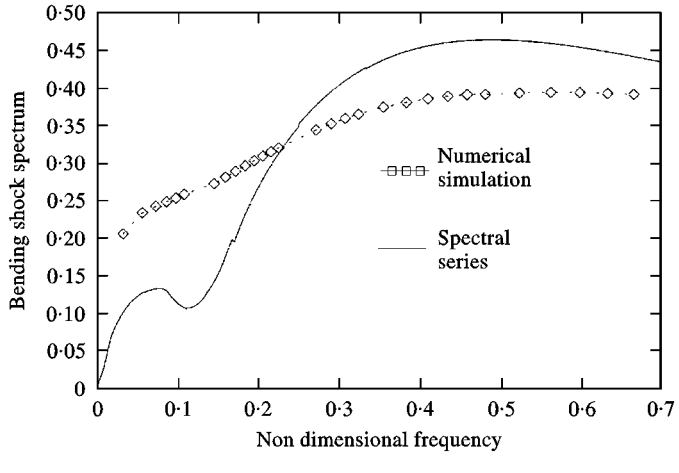

Figure 8. Comparison between the theoretical and the numerical maximum bending moment for $\tilde{f}_e = 0{\cdot}16$: numerical ◇-◇-◇, simulation; —— spectral series.

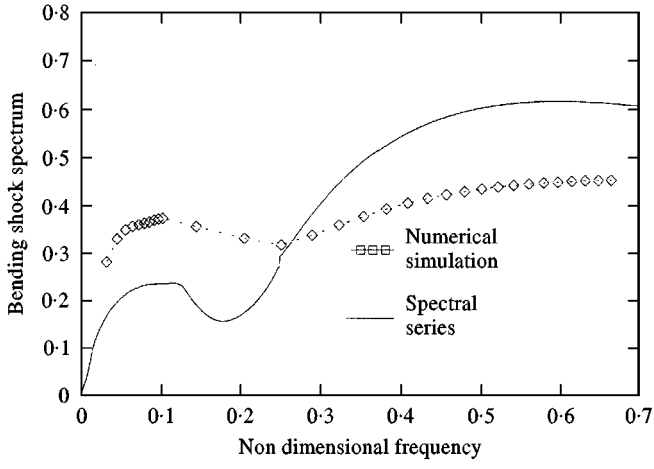

Figure 9. Comparison between the theoretical and the numerical maximum bending moment for $\tilde{f}_e = 0{\cdot}25$: numerical ◇-◇-◇, simulation; ——, spectral series.

The differences can be attributed mainly to some hypotheses used in deriving the spectral series. In particular, the pressure load has been replaced by a rectangular travelling load and the bending moment has been obtained by the approximate relationship (13). The first assumption is made for simplicity, while the second one is needed because the spectral series, obtained by the exact expression of the bending moment, does not converge.

4. NUMERICAL ANALYSIS OF THE HYDRODYNAMIC FORCE

In this section the analysis of the hydrodynamic problem of water entry is developed following a more sophisticated model, similar to that described in reference [10], but here coupled with the dynamics of the 2 d.o.f. elastic system described in section 3.1. Thus the present hydrodynamic model accounts for a variable drop velocity and for the hydroelastic coupling. In this case, the theoretical formulation accounts for the free surface deformation, neglected in the model developed in section 2 based on the plate potential theory [9], leading to a non-linear moving boundary problem. Of course in this case the results cannot be obtained in closed form but a numerical procedure provides the expected hydrodynamic force.

The flow is assumed irrotational and the fluid inviscid, so that the velocity field can be expressed in terms of the velocity potential ϕ that satisfies the Laplace equation. This equation is solved by means of a boundary element formulation in a computational domain limited by the body contour S_B and the free surface S_F. By introducing the two-dimensional free space Green's function of the Laplace operator G, at any point x inside the computational domain the velocity potential is

$$\phi(x) = \int_S \left[\frac{\partial \phi}{\partial v_n}(y) G(x-y) - \phi(y) \frac{\partial G}{\partial v_n}(x-y) \right] \mathrm{d}S(y), \tag{15}$$

where v_n is the unit vector normal to the boundary, oriented inward to the fluid domain and $S = S_B \cup S_F$. Equation (15) describes completely the flow field $\mathbf{u} = \nabla\phi$ once the velocity potential and its normal derivative are known throughout S.

Due to the impermeability constraint, the normal derivative of ϕ is assigned to the body contour while, on the free surface, the velocity potential is updated according to the unsteady Bernuolli equation. Actually, the pressure on the free surface is assumed to be constant and, due to the kinematic condition, the Bernoulli equation reads

$$\frac{\mathrm{D}\phi}{\mathrm{D}t} = g\zeta + \frac{|\nabla\phi|^2}{2}, \tag{16}$$

where ζ is the vertical co-ordinate, positive downwards, with $\zeta = 0$ on the undisturbed water surface. In the initial phase of the impact the kinematic contribution to the right-hand side of equation (16) is much stronger than the gravity term, and hence the latter is usually neglected in using that equation. As an initial condition to equation (16), $\phi = 0$ is assumed on the free surface. It should be remarked that this initial condition implies a zero tangential velocity along the free surface and, as a consequence, the limit of the velocity field, from the free surface inward the body, violates the impermeability constraint. This is due to the neglected surface tension effects that would avoid the discontinuity of the normal vector at the intersection between the free surface and the body.

The velocity potential on S_B and its normal derivative on S_F are determined by solving the integral equation, obtained by applying equation (15) on the boundary of the fluid domain S. Once the velocity potential along the body surface is known, the dynamic pressure is computed by the unsteady Bernoulli equation.

The problem stated above is numerically solved with a scheme similar to that employed in reference [10] that is briefly described in the following. The boundary at the fluid domain is discretized with segments on which the velocity potential and its normal derivative are assumed to be constant and equal to the value they take at the centroid. The boundary integral equation is solved by providing the velocity potential on the body contour and its normal derivative on the free surface. A second order Runge–Kutta scheme is employed for the integration of motion of midpoints on the free surface and of the velocity potential above it. A cubic spline is used to reconstruct the vertices distribution. For the sake of accuracy, at each time step, the panel distribution is refined in highly curved regions.

In the potential approximation the solution of the problem is highly challenging due to the velocity singularity occurring at the intersection between the free surface and the body contour [24]. This singularity in the velocity field leads to the formation of a water jet that needs a suitable procedure to be described numerically. Some aspects of this procedure are given below but more details can be found in reference [10] that originally suggested the model.

In a first stage of the numerical simulation the free surface is assumed to intersect the body. Successively, a thin water jet develops, characterized by a strong velocity

gradient normal to the body. An accurate description of the development of the jet region would require an increasing number of elements of smaller dimensions and, as a consequence, a dramatic reduction of the time step. For this reason when the distance between the midpoint of the first panel on the free surface and the body contour becomes smaller than a cut-off length, the first panel is replaced by a straight line panel P normal to the body surface. In order to match both the body and the free surface boundary conditions a linear variation of the velocity potential is assumed along this panel. The tangential derivatives is equal to the normal derivative assigned to the body contour while the velocity potential is assigned to the free surface side.

During the time integration, whenever the first panel on the free surface beyond P forms an angle with the body contour smaller than a limit value (usually 2°), it is excluded and the jet truncation is moved back.

Before applying the numerical procedure to the impact of elastic systems, the water entry of a wedge with a deadrise angle of 10° has been simulated for a constant drop velocity. After a transient phase, in which the jet develops, a similarity solution is achieved.

At each time step the solution of the fluid dynamic problem provides the hydrodynamic load F_h used as the forcing term of the dynamic equation when analyzing the impact on the 2 d.o.f.s elastic system. Thus, the problem is solved coupling the equations of the hydrodynamic field and the equations of the two elastically connected masses freely dropping into the water. The solution found provides, at each time step, the new impacting body configuration and the associated velocity that are used to update the boundary conditions.

Due to the treatment of the jet region, strong oscillations characterize the slamming load and a suitable filter has been applied to the numerical results.

5. CONCLUSIONS

In this paper, the problem of the impact of an elastic system on the water is investigated. The main point is related to a particular shock spectral approach, that allows one to avoid a direct solution of the problem. In this way, an *a priori* estimate of the elastic response of the systems in terms of the characteristic dimensionless parameters of the phenomenon is obtained. However under some simplified hypotheses, the comparison with both experimental and numerical simulations confirms that the proposed analysis provides a very accurate estimate of the elastic force excited by the water impact.

The procedure has a rather general character and it does not seem too difficult to apply this technique to more complex structures even when described by a finite element method.

ACKNOWLEDGMENT

This work was supported by the Ministero dei Trasporti della Navigazione in the frame of INSEAN research program 1997–99.

REFERENCES

1. R. E. D. Bishop and W. G. Price 1979 *Hydroelasticity of Ships*. Cambridge: University Press.
2. R. E. D. Bishop, W. G. Price and Y. Wu 1986 *Philosophical Transactions of Royal Society of London* **A 316**, 375–426. A general linear hydroelasticity theory of floating structures moving in a seaway.
3. W. G. Price, P. Temarel and A. J. Keane 1994 *Hydroelasticity in Marine Technology*, *Hydroelastic Analysis of a SWATH in Waves* (Faltinsen editor), 231–243. Rotterdam: Balkema.
4. A. Korobkin and V. V. Pukhnachov 1998 *Annual Review in Fluid Mechanics* **20**, 159–185. Initial stage of water impact.
5. O. M. Faltinsen 1997 *Philosophical Transactions of the Royal Society of London* **A 355**, 575–591. The effect of hydroelasticity on ship slamming.
6. R. Skalak and D. Feit 1966 *Transactions ASME B*: *Journal of Engineering for Industry* **88**, 325–331. Impact on the surface of a compressible fluid.
7. A. Korobkin 1992 *Journal of Fluid Mechanics* **244**, 437–453. Blunt-body impact on a compressible liquid surface.
8. T. Von Karman 1929 *NACA TN* 321. The impact of seaplane floats during landing.
9. H. Wagner 1932 *Z. Angew. Math. Mech.* **12**, 192–215. Uber stoss und Gleitvorgange an der Oberflache von Flussigkeiten.
10. R. Zhao and O. Faltinsen 1993 *Journal of Fluid Mechanics* **246**, 593–612. Water entry of two-dimensional bodies.
11. R. Zhao and O. Faltinsen 1998 *Proceedings of the 22nd Symposium on Naval Hydrodynamics Washington*, DC, U.S.A. Water entry to axisymmetric bodies with and without flow separation.
12. L. Xu, A. W. Troesh and W. S. Vorus *Journal of Ship Research* **42**, 187–198. Asymmetric vessel impact and planing hydrodynamics.
13. D. J. Kim, W. Vorus, A. Troesh and R. Gollwitzer 1996 *Proceedings of the 21st Symposium on Naval Hydrodynamics*, *Trondheim*, *Norway*. Coupled hydrodynamic impact and elastic response.
14. J. Klasvold and O. Faltinsen 1995 *Journal of Ship Research* **39**, 225–239. Hydroelastic modelling of wet deck slamming on multihull vessel.
15. W. S. Vorus 1996 *Journal of Ship Research* **40**, 89–106. A flat cylinder theory for vessel impact and steady planning resistance.
16. A. Iafrati, A. Carcaterra, E. Ciappi and E. Campana 1998 *Proceedings of the 2nd International Conference on Hydroelasticity in Marine Technology*, *Fukuoka*, *Japan*. (Kashiwagi et al., editors), 129–138. Impact of rigid and elastic systems over the water surface.
17. A. Carcaterra and E. Ciappi 1999 *Nonlinear Dynamics*. Prediction of the compressible stage slamming force on rigid and elastic systems impacting on the water surface (submitted).
18. W. H. Chu and H. N. Abramson 1961 *Journal of Ship Research* Hydrodynamic theories of ship slamming-review and extension.
19. Z. N. Dobrovol' Skaya 1969 *Journal of Fluid Mechanics* **36**, 805–829. On some problems of similarity flow of fluid with a free surface.
20. L. Meirovitch 1986 *Elements of Vibration Analysis*. New York: McGraw-Hill
21. J. T. Broch 1980 *Mechanical Vibration and Shock Measurements*. Denmark: B & K.
22. A. Carcaterra and A. Sestieri 1995 *Journal of Sound Vibration* **188**, 205–233. Complex envelope displacement analysis: a quasi-static approach to vibrations.
23. G. P. Tolstov *Fourier Series*. New York: Dover Publications.
24. M. Greenhow and W. M. Lin 1985 *Proceedings of the 4th International Conference on Numerical Ship Hydrodynamics*, *Washington*, DC, U.S.A. Numerical simulation of nonlinear free surface flows generated by wedge entry and wavemaker motions.

APPENDIX A

The basic property of the Hilbert trasform holds: $\mathscr{H}\{\sin p\,t\} = -\cos pt$. Therefore, the analytical signal $\hat{q}_k = q_k + \mathrm{j}\mathscr{H}\{q_k\}$, is simply

$$\hat{q}_k(t) = \frac{1}{\omega_k}\int_{-\infty}^{+\infty} I_k(\tau)\,[\sin\omega_k(t-\tau) - \mathrm{j}\cos\omega_k(t-\tau)]\,\mathrm{d}\tau$$

$$= -\frac{\mathrm{j}}{\omega_k}\int_{-\infty}^{+\infty} I_k(\tau)\,\mathrm{e}^{\mathrm{j}\omega_k(t-\tau)}\,\mathrm{d}\tau = -\frac{\mathrm{j}}{\omega_k}\,\mathrm{e}^{\mathrm{j}\omega_k t}\int_{-\infty}^{+\infty} I_k(\tau)\,\mathrm{e}^{-\mathrm{j}\omega_k\tau}\,\mathrm{d}\tau$$

which proves the required result.

APPENDIX B

Starting from the analytic signal

$$\hat{q}_k(t) = -\frac{\mathrm{j}}{\omega_k}\,\mathrm{e}^{\mathrm{j}\omega_k t}\int_{-\infty}^{+\infty} I_k(\tau)\,\mathrm{e}^{-\mathrm{j}\omega_k\tau}\,\mathrm{d}\tau = -\frac{\mathrm{j}}{2\pi f_k}\,\mathrm{e}^{2\pi\mathrm{j}f_k t}\int_{-\infty}^{+\infty} I_k(\tau)\,\mathrm{e}^{-2\pi\mathrm{j}f_k\tau}\,\mathrm{d}\tau$$

and recalling that

$$f_k = \tilde{f}_k/t^* = k^2\tilde{f}_1/t^*, \quad \tau = \tilde{\tau}\,t^*$$

and

$$I_k = F^*\sqrt{2/m_p}\,\tilde{I}_k = F^*\sqrt{2/m_p}\,\frac{\tilde{F}_h(\tilde{t})}{\pi k}\left(\frac{(-1)^k - 1}{\alpha} + \frac{1}{4\tilde{f}_e\tilde{t}}\,[1 - \cos 2\pi k\,\tilde{f}_e\,\tilde{t}]\right)$$

thus

$$\hat{q}_k(t) = -\frac{j}{2\pi k^2\tilde{f}_1}\,t^*\,\mathrm{e}^{2\pi\mathrm{j}k^2\tilde{f}_1\tilde{t}}\,F^*\sqrt{2/m_p}\int_{-\infty}^{+\infty}\tilde{I}_k(\tilde{\tau})\,e^{-2\pi jk^2\tilde{f}_1\tilde{\tau}}\,\mathrm{d}\tilde{\tau}\,t^*$$

$$= -\frac{\mathrm{j}}{2\pi k^2\,\tilde{f}_1}\,(F^*\,t^*)\,t^*\,\sqrt{2/m_p}\,\mathrm{e}^{2\pi\mathrm{j}k^2\tilde{f}_1\tilde{t}}\,\tilde{\mathscr{F}}_k\{\tilde{I}_k\}\,.$$

By substituting $F^*\,t^* = 20/81\,mv_0 = 20/81\,\alpha m_p v_0$ and $t^* = 16/15\,(\zeta^*/v_0)$ into the previous relationship the following equation holds:

$$\hat{q}_k(t) = -\sqrt{m_p}\,\zeta^*\,\frac{\mathrm{j}\,\mathrm{e}^{2\pi\mathrm{j}k^2\tilde{f}_1\tilde{\tau}}}{2\pi k^2\tilde{f}_1}\,\frac{64}{243}\,\sqrt{2}\,\tilde{\mathscr{F}}_k\{\tilde{I}_k\}.$$

APPENDIX C

Using the relationship

$$M_B \approx \pi^2\,\frac{D}{L^2}\,\zeta_e \leqslant \pi^2\,\frac{D}{L^2}\,|\tilde{\zeta}_e|\,\zeta^* = \pi^2\,\frac{D}{L^2}\,|\tilde{\zeta}_e|\,\frac{15}{16}\,v_0\,t^*$$

and since

$$\tilde{f}_1^2 = \frac{D}{\rho_s h}\frac{\pi^2}{(2L^2)^2}\,t^{*2}, \qquad t^* = \frac{16}{15}\sqrt{\frac{2\alpha m_p}{5\pi\rho_a\gamma}}\frac{\operatorname{tg}\beta}{v_0}, \qquad m_p = \rho_S h L,$$

$$|\tilde{\bar{\zeta}}_e| \leqslant \frac{\pi}{2}\frac{\varepsilon\alpha}{2\pi f_1}\sqrt{\sum_{k=1}^{\infty}|z_k|^2},$$

after some mathematics, one obtains

$$|\tilde{M}_B| = \left|\frac{\hat{M}_B}{p_0 L^2}\right| \leqslant 10\,\pi\left(\frac{15}{16}\right)^3 \varepsilon\frac{\sqrt{\gamma}}{\operatorname{tg}\beta}\,\tilde{f}_1\tilde{f}_e\sqrt{\sum_{k=1}^{\infty}|z_k|^2},$$

where $\tilde{M}_B$ is the non-dimensional bending moment, h is the plate's thickness and $p_0 = 0{\cdot}5\,\rho_w v_0^2$.

When z_k is given in explicit form, and the frequency $\tilde{f}_1$ is carried under the square root, one finally has $|z_k| = |\tilde{\mathscr{F}}_k\{\tilde{I}_k\}|/k$, and thus

$$|\tilde{M}_B| \leqslant 10\pi\left(\frac{15}{16}\right)^3 \varepsilon\frac{\sqrt{\gamma}}{\operatorname{tg}\beta}\,\tilde{f}_e\sqrt{\sum_{k=1}^{\infty}\frac{|\tilde{\mathscr{F}}_k\{\tilde{I}_k\}|^2\;(2\pi k^2\tilde{f}_1)}{4\pi^2 k^6}} = 5\left(\frac{15}{16}\right)^3 \varepsilon\frac{\sqrt{\gamma}}{\operatorname{tg}\beta}\,\tilde{f}_e\sqrt{\sum_{k=1}^{\infty}\frac{\tilde{S}_k}{k^6}},$$

where the shock spectral components are defined as $\tilde{S}_k = 2\pi\tilde{f}_k|\tilde{\mathscr{F}}_k\{\tilde{I}_k\}|$.

APPENDIX D

The shock spectral component needs the computation of the Fourier tranform of the function $\tilde{I}_k$. Therefore,

$$\tilde{\mathscr{F}}_k[\tilde{I}_k\} = \tilde{\mathscr{F}}_k\left\{\frac{(-1)^k-1}{\pi\alpha k}\,\tilde{F}_h(\tilde{t}) + \frac{1}{4\pi k\tilde{f}_e}\frac{\tilde{F}_h(\tilde{t})}{\tilde{t}} - \frac{1}{4\pi k\tilde{f}_e}\frac{\tilde{F}_h(\tilde{t})}{\tilde{t}}\cos 2\pi k\tilde{f}_e\tilde{t}\right\},$$

so that

$$\tilde{\mathscr{F}}_k\{\tilde{I}_k\} = \frac{(-1)^k-1}{\pi\alpha k}\,\tilde{\mathscr{F}}_k\{\tilde{F}_h(\tilde{t})\} + \frac{1}{4\pi k\tilde{f}_e}\,\tilde{\mathscr{F}}_k\left\{\frac{\tilde{F}_h(\tilde{t})}{\tilde{t}}\right\}$$

$$-\frac{1}{4\pi k\tilde{f}_e}\,\tilde{\mathscr{F}}_k\left\{\frac{\tilde{F}_h(\tilde{t})}{\tilde{t}}\right\} * \tilde{\mathscr{F}}_k\{\cos 2\pi k\tilde{f}_e\tilde{t}\}$$

or

$$\tilde{\mathscr{F}}_k\{\tilde{I}_k\} = \frac{(-1)^k-1}{\pi\alpha k}\,\tilde{\mathscr{F}}_k^{(I)}(\tilde{f}_k) + \frac{1}{4\pi k\tilde{f}_e}\,\tilde{\mathscr{F}}_k^{(T)}(\tilde{f}_k)$$

$$-\frac{1}{4\pi k\tilde{f}_e}\,\tilde{\mathscr{F}}_k^{(T)}(\tilde{f}_k) * \tilde{\mathscr{F}}_k\{\cos 2\pi k\tilde{f}_e\tilde{t}\}$$

where prime (I) and (T) denote the inertial and the travelling contribution, respectively. Since

$$\tilde{\mathscr{F}}_k\{\cos 2\pi k\tilde{f}_e\tilde{t}\} = \frac{1}{2}[\delta(k^2\tilde{f}_1 - k\tilde{f}_e) + \delta(k^2\tilde{f}_1 + k\tilde{f}_e)]$$

thus

$$\tilde{\mathscr{F}}_k\{\tilde{I}_k\} = \frac{(-1)^k - 1}{\pi\alpha k}\,\tilde{\mathscr{F}}_k^{(I)}(\tilde{f}_k) + \frac{1}{4\pi k\,\tilde{f}_e}\,\tilde{\mathscr{F}}_k^{(T)}(\tilde{f}_k) - \frac{1}{4\pi k\,\tilde{f}_e}\,\frac{1}{2}\,\{\tilde{\mathscr{F}}_k^{(T)}(\tilde{f}_k - k\tilde{f}_e) + \tilde{\mathscr{F}}_k^{(T)}(\tilde{f}_k + k\tilde{f}_e)\}.$$

Therefore, the final expression is

$$\tilde{S}_k(\alpha, \tilde{f}_1, \tilde{f}_e) = \left| \frac{(-1)^k - 1}{\pi\alpha k}\,\tilde{S}^{(I)}(\tilde{f}_k) + \frac{1}{4\pi k\tilde{f}_e}\,\tilde{S}^{(T)}(\tilde{f}_k) - \frac{1}{8\pi k\,\tilde{f}_e}\left[\frac{\tilde{S}^{(T)}(\tilde{f}_k + k\tilde{f}_e)}{1 + \tilde{f}_e/(k^2\,\tilde{f}_1)} + \frac{\tilde{S}^{(T)}(\tilde{f}_k - k\,\tilde{f}_e)}{1 - \tilde{f}_e/(k^2\,\tilde{f}_1)}\right]\right|$$

leading to the natural definitions of the complex inertial shock spectrum $\bar{S}^{(I)}$ and travelling shock spectrum $\tilde{S}^{(T)}$:

$$\tilde{S}^{(1)}(p) = 2\pi p\tilde{\mathscr{F}}\{\tilde{F}_h\}, \qquad \tilde{S}^{(T)}(p) = 2\pi p\tilde{\mathscr{F}}\{\tilde{F}_h/\tilde{t}\}, \qquad \tilde{\mathscr{F}}(\cdot) = \int_{-\infty}^{+\infty} (\cdot)\,\mathrm{e}^{-2\pi\mathrm{j}p\tilde{t}}\,\mathrm{d}\tilde{t}.$$

APPENDIX E

$$\tilde{S}_k(\alpha, \tilde{f}_1, \tilde{f}_e) = \left| \frac{(-1)^k - 1}{\pi\alpha k}\,\tilde{S}^{(I)}(\tilde{f}_k) + \frac{1}{4\pi k\,\tilde{f}_e}\,\tilde{S}^{(T)}(\tilde{f}_k) - \frac{1}{8\pi k\,\tilde{f}_e}\left[\frac{\tilde{S}^{(T)}(\tilde{f}_k + k\tilde{f}_e)}{1 + \tilde{f}_e/(k^2\,\tilde{f}_1)} + \frac{\tilde{S}^{(T)}(\tilde{f}_k - k\,\tilde{f}_e)}{1 - \tilde{f}_e/(k^2\,\tilde{f}_1)}\right]\right|,$$

$$\tilde{S}_{OV_k}(\alpha, \tilde{f}_1, \tilde{f}_e) = \left| \frac{(-1)^k - 1}{\pi\alpha k}\,\tilde{S}_{OV}^{(I)}(\tilde{f}_k)\right| - \left|\frac{1}{4\pi k\,\tilde{f}_e}\,\tilde{S}^{(T)}(\tilde{f}_k) - \frac{1}{8\pi k\,\tilde{f}_e}\left[\frac{\tilde{S}^{(T)}(\tilde{f}_k + k\tilde{f}_e)}{1 + \tilde{f}_e/(k^2\,\tilde{f}_1)} + \frac{\tilde{S}^{(T)}(\tilde{f}_k - k\,\tilde{f}_e)}{1 - \tilde{f}_e/(k^2\,\tilde{f}_1)}\right]\right|,$$

$$|\tilde{M}_B| = 5\left(\frac{15}{16}\right)^3 \varepsilon\frac{\sqrt{\gamma}}{\mathrm{tg}\,\beta}\,\tilde{f}_e\,\sqrt{\sum_{k=1}^{\infty}\frac{\tilde{S}_k}{k^6}}, \qquad |\tilde{M}_{BOV}| = 5\left(\frac{15}{16}\right)^3 \varepsilon\frac{\sqrt{\gamma}}{\mathrm{tg}\,\beta}\,\tilde{f}_e\,\sqrt{\sum_{k=1}^{\infty}\frac{\tilde{S}_{OV\,k}}{k^6}},$$

$$|\tilde{M}_{AV}| = \tfrac{1}{2}\,(|\tilde{M}_{BOV}| + |\tilde{M}_B|).$$

APPENDIX F

A rough estimate of θ due to the combined effect of the inertial and pressure loads is obtained. They can be assimilated to pulse actions of characteristics time duration t^*, at least when the structure natural period is large than t^* (i.e., if $\tilde{f}_1 < 1$).

The plate deflection under an inertial load of amplitude F^*/L, accounting only for the first mode response, is

$$\zeta_{ei} \approx \frac{2}{\alpha}\sqrt{\frac{2}{m_p}}\frac{F^* t^*}{\pi(2\pi f_1)}\,\Phi_1(x)\sin(2\pi f_1\, t),$$

thus

$$\theta_{i\max}|_{x=0} \propto \frac{m v_0}{\alpha m_p f_1 L} \;\Rightarrow\; \theta_{i\max}|_{x=0} \;\propto\; \frac{v_0}{f_1\, L}.$$

The pressure load is assimilated again to an impulse of amplitude F^* of time duration t^* applied at the abscissa $v_e t^*$ (the bound of the wetted area at the instant in which the maximum force occurs). By assuming only the first mode response at the beam midpoint, the maximum elastic deflection due to the pressure load is

$$\zeta_{ep} = \sqrt{\frac{2}{m_p}}\frac{F^* t^*}{2\pi f_1}\sin\left(\frac{\pi v_e t^*}{L}\right)\Phi_1(x)\sin(2\pi f_1\, t).$$

When $\tilde{f}_e \ll 1$ (see condition (ii)), the following approximation holds: $\sin(\pi v_e t^*/2L) \approx \pi v_e t^*/2L$. After some mathematics one has

$$\theta_{p\max} \;\propto\; \frac{\alpha v_0}{L f_1}\frac{v_e t^*}{L}.$$

Since the inertial and the pressure loads act in opposite direction, the total slope is estimated as

$$\theta_{\max} = |\theta_{i\max} - \theta_{p\max}| = \left|\alpha\frac{v_0}{L f_1}\frac{v_e}{L} - \frac{v_0}{f_1\, L}\right|.$$

Thus, the applicability of the developed analysis is subjected to the condition

$$\theta_{\max} \ll \beta \;\Rightarrow\; \tilde{f}_e\,|1 - \alpha\,\tilde{f}_e| \ll \tilde{f}_1.$$